Chem

CellPress

Article

Transparent-to-Dark Electrochromic Behavior in Naphthalene-Diimide-Based Mesoporous MOF-74 Analogs

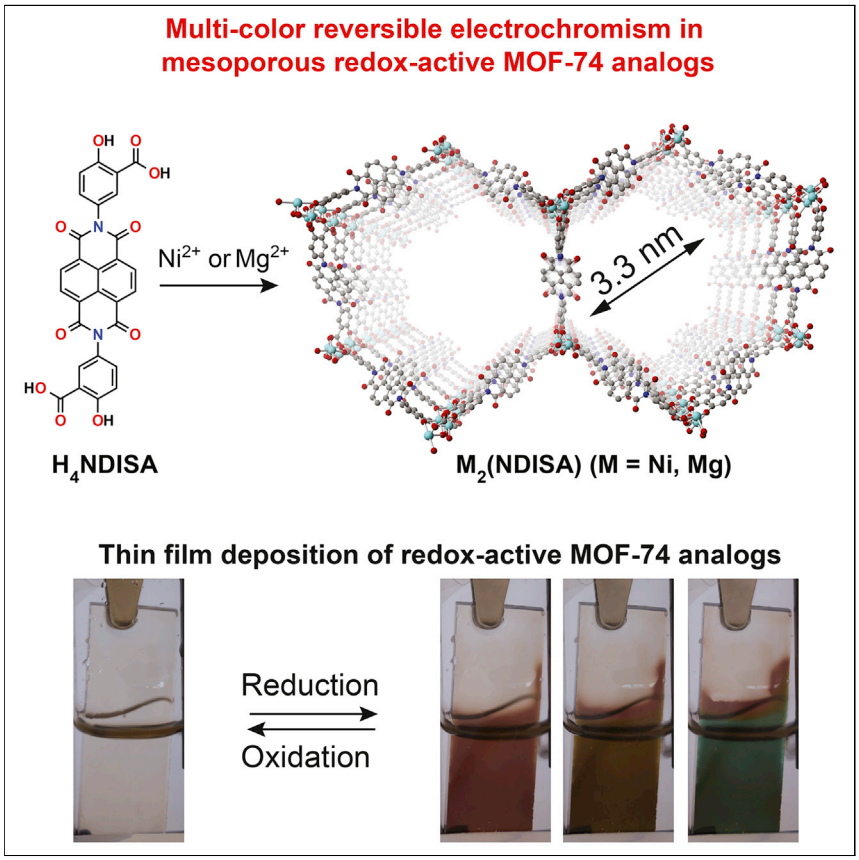

Dincă and colleagues show that incorporating a naphthalene-diimide-based ligand into a MOF affords the synthesis of redox-active, mesoporous MOF-74 analogs that display fast and reversible electrochromic switching from transparent to dark. The authors devised techniques that allow for the deposition of these new materials as thin films, whose morphology affects the electrochromic response.

Khalid AlKaabi, Casey R. Wade, Mircea Dincă

mdinca@mit.edu

HIGHLIGHTS

Synthesis of the first redox-active mesoporous MOF-74 analog

Strategies for thin-film deposition of the MOFs on FTO were developed

The MOFs display reversible electrochromic switching from transparent to dark

AlKaabi et al., Chem 1, 264–272
August 11, 2016
http://dx.doi.org/10.1016/j.chempr.2016.06.013

Chem

CellPress

Article

Transparent-to-Dark Electrochromic Behavior in Naphthalene-Diimide-Based Mesoporous MOF-74 Analogs

Khalid AlKaabi,[1] Casey R. Wade,[1] and Mircea Dincă[1,2,*]

SUMMARY

The deliberate insertion of redox-active naphthalene diimide ligands into the versatile family of metal-organic frameworks known as MOF-74 (CPO-27) gives rise to a mesoporous electrochromic MOF that can be switched from transparent to dark, a desirable feature in electrochromic devices such as smart windows. Specifically, we report two new materials that have the MOF-74 topology and display redox activity stemming from a naphthalene diimide salicylic acid (NDISA) ligand. We show that these materials can be deposited as thin films on fluorine-doped tin oxide glass. The surprisingly different morphologies of MOF films obtained from Mg^{2+} and Ni^{2+} ions is likely controlled by the nucleation kinetics of Mg_2(NDISA) and Ni_2(NDISA), respectively. Both materials exhibit well-behaved quasi-reversible redox events associated with the [NDI]/$[NDI]^{\cdot-}$ and $[NDI]^{\cdot-}$/$[NDI]^{2-}$ redox couples, which are also responsible for the electrochromic switching.

INTRODUCTION

Tuning the electronic structure of metal-organic frameworks (MOFs) by incorporating redox-active components is a powerful strategy for expanding the functionality of this class of compounds. This approach can give rise to materials with enhanced performance in applications such as electrocatalysis,[1,2] photo- and electrochromism,[3–7] and devices made from conductive MOFs.[8–11] Although MOFs offer a high degree of structural and compositional tunability, which makes them attractive for the design of optoelectronic devices, their implementation in such devices is partly limited by the inherent difficulty associated with their processing.[8–12] Indeed, most MOFs are obtained as insoluble microcrystalline powders,[13] and the development of processing methods, such as thin-film deposition, must be pursued in congruence with the development of new physical properties, such as electrochromism.[14] Here, we demonstrate that naphthalene diimide (NDI), a redox-active molecule whose optical properties change with the redox state, can be substituted with salicylic acid groups to yield MOFs with the same topology as the well-known MOF-74.[15–18] This class of materials can be expanded isoreticularly without pore collapse, and here, too, we observed a pore size reaching the mesoporous regime, which is beneficial for electrolyte transport in the context of electrochromism. Although MOFs in the MOF-74 family can show ligand-based redox activity, this is usually associated with the oxidation of the phenol group that ligates the secondary building unit; this oxidation weakens the M–O bond and can compromise structural integrity.[17,18] Here, we show that use of the NDI ligand leads to well-defined reversible redox couples that are also responsible for fast transparent-to-dark optical switching, a desirable feature in electrochromic devices.

The Bigger Picture

Electrochromic materials, which change color or light absorption with the application of current, are poised to change the landscape of energy efficiency, especially in the form of smart windows. Several technical targets must be met in the consideration of new candidates for electrochromic materials. These include color, switching time, and processability as thin films. With their tunable chemical composition and structure, metal-organic frameworks (MOFs) are prime candidates for electrochromic materials. Here, we show that inserting naphthalene diimide, a known color-changing organic compound, into MOF-74, a MOF with hexagonal channels, creates a material that has large mesopores and exhibits fast and reversible switching from transparent to dark. This work describes the first example of a redox-active mesoporous MOF-74 analog, a class of materials that is prominent in the field. It could thus inspire broader applications of redox-active MOFs in other renewable-energy applications, including energy-storage devices and catalysis.

Owing to their electron-deficient and aromatic nature, as well as their facile functionalization, NDIs have been extensively investigated as *n*-type semiconductors in organic electronics.[19–21] Because functionalization of the NDI core leads to derivatives that can absorb the full visible spectrum,[19] these molecules have been used in MOF-based applications that target optical reading of an input or analyte, such as sensing[22,23] and electro- or photochromism.[3–7] However, many NDI-based MOFs feature topologies that are prone to interpenetration and/or exhibit metal-dependent polymorphism. This is problematic when optical output is important, because the absorption and emission spectra can be influenced by excitonic coupling processes as a result of the relative proximity of NDI cores. Furthermore, interpenetration generally reduces pore aperture and can impede electrolyte transport in electrochromic applications. We surmised that incorporating NDI-based linkers in mesoporous materials with the MOF-74 topology would provide solutions for both of these challenges while allowing for reversible redox activity in an otherwise robust set of materials.

RESULTS

Condensation of 5-amino-2-hydroxybenzoic acid with 1,4,5,8-naphthalenetetracarboxylic dianhydride in *N*,*N*-dimethylformamide (DMF) produced *N*,*N*′-bis(3-carboxy-4-hydroxyphenyl)-1,4,5,8-naphthalenetetradicarboximide (NDI-bis-salicylate, H_4NDISA) in a 70% yield (Scheme S1). Subsequent reaction of H_4NDISA with $Mg(NO_3)_2{\cdot}6H_2O$ or $Ni(NO_3)_2{\cdot}6H_2O$ in a mixture of DMF, ethanol, and water at 120°C for 1 day resulted in the precipitation of $[Mg_2(NDISA)(H_2O)_2]{\cdot}2.4(H_2O)$ (**Mg-NDISA**) or $[Ni_2(NDISA)(H_2O)_2]{\cdot}4(H_2O)$ (**Ni-NDISA**) as a dark-orange or brown microcrystalline powder, respectively. Powder X-ray diffraction (PXRD) patterns of materials dried with supercritical CO_2 matched those simulated from model structures predicted on the basis of the known MOF-74 topology (Figures 1 and 2). Pawley refinement for both materials was performed against the experimental PXRD patterns (R_{wp} = 5.90%–7.98%; see Figure S1 and Table S1), and it was found that the MOFs crystallized in trigonal space groups with lattice parameters $a = b \sim 59$ Å.[24] The *c* parameter was not refined as a result of the low observed intensity of high-angle peaks; however, we do not expect it to deviate significantly from the values reported in other frameworks with the MOF-74 topology (i.e., $c \sim 6.5$ Å).[15–18] As expected, the structures exhibited one-dimensional channels with a pore diameter of approximately 3.3 nm (no solvent molecules were included in the model). Importantly, these mesopores should facilitate ion and electrolyte transport during electrochromic cycling.

Mg-NDISA and **Ni-NDISA** exhibit different morphologies when deposited as thin films. When **Mg-NDISA** is grown on fluorine-doped tin oxide (FTO) glass under conditions mimicking its bulk synthesis, only thick, non-uniform powders are deposited. However, uniform films of **Mg-NDISA** can be deposited on FTO using an anhydrous mixture of DMF and methanol at 120°C, as confirmed by PXRD analysis (Figures 2 and S2). Scanning electron microscopy revealed a fiber-like morphology for these films, with features as thin as approximately 25 nm. This morphology contrasts with that observed for **Ni-NDISA** films, which were much denser and more uniform, despite having been deposited under conditions identical to those of the **Mg-NDISA** films. Clearly, the difference in morphology stems from the different rates of nucleation and growth for the two materials: the Ni material likely nucleates much faster and thus produces denser films than its Mg analog, whose growth appears to dominate overall film deposition. Faster nucleation may also be responsible for rapid precipitation of **Ni-NDISA**, which can be isolated within approximately 15 min, whereas

[1]Department of Chemistry, Massachusetts Institute of Technology, 77 Massachusetts Avenue, Cambridge, MA 02139, USA

[2]Lead Contact

*Correspondence: mdinca@mit.edu

http://dx.doi.org/10.1016/j.chempr.2016.06.013

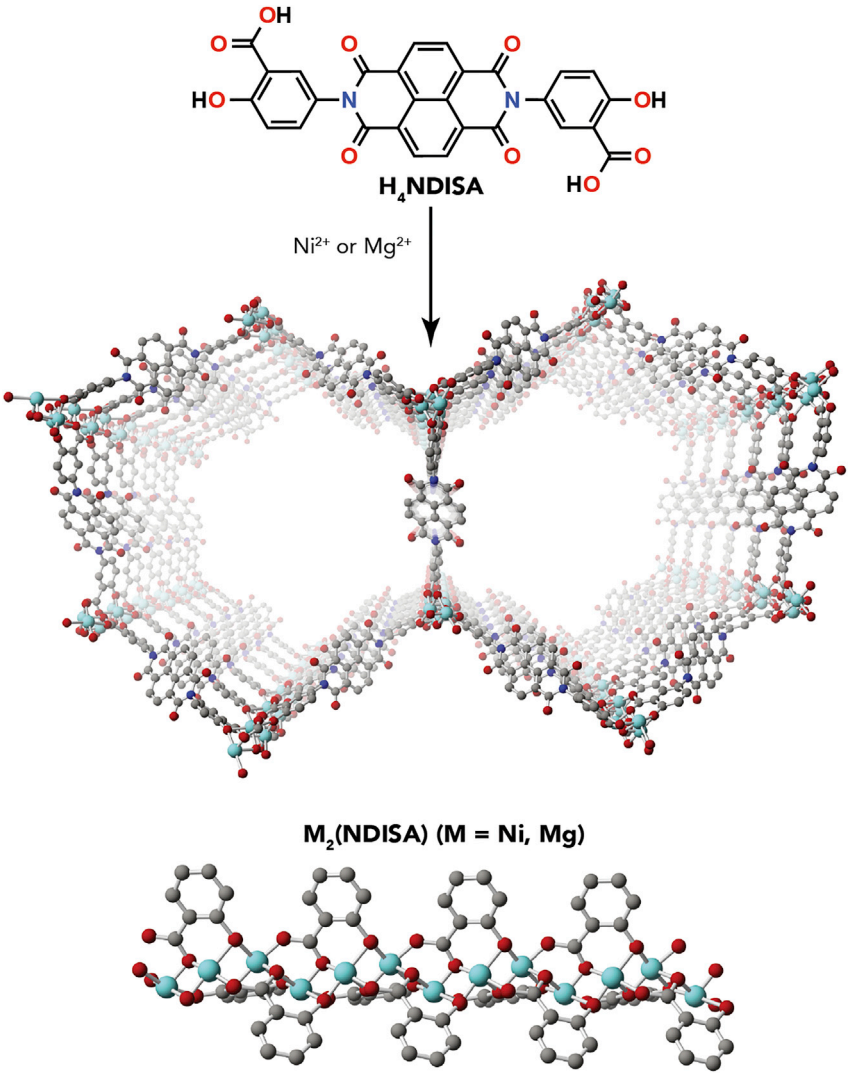

Figure 1. Synthesis and Simulated Structure of M-NDISA along the *c* Axis
A representation of the secondary building unit is shown. Teal, blue, red, and gray spheres represent metal (Mg or Ni), N, O, and C atoms, respectively. H atoms are omitted for clarity.

Mg-NDISA requires an induction period of at least 40 min. The different relative rates of nucleation and growth for the two materials, which affect the morphology of their thin films, have a profound effect on the optical properties of the films, as discussed below.

Both Mg-NDISA and Ni-NDISA films exhibit two quasi-reversible one-electron redox couples (Table 1 and Figure S3). The first and second reduction peaks are consistent with the formation of the radical anion $[NDI]^{\cdot-}$ and dianion $[NDI]^{2-}$, respectively. The cathodic shift in the reduction potentials observed for the thin films in relation to the free ligand (Table 1 and Figure S4) could be due to the immobilization of the ligand inside the MOF or differences between solution and solid-state kinetics, as brought about either by electrolyte diffusion limitations or by electron hopping within the MOF skeleton. Nevertheless, attesting to the stability of the new MOFs to redox reactivity, both films showed excellent stability to cyclic voltammetry (CV), and there was no observable decrease in crystallinity up to ten cycles (see Figures S5 and S6).

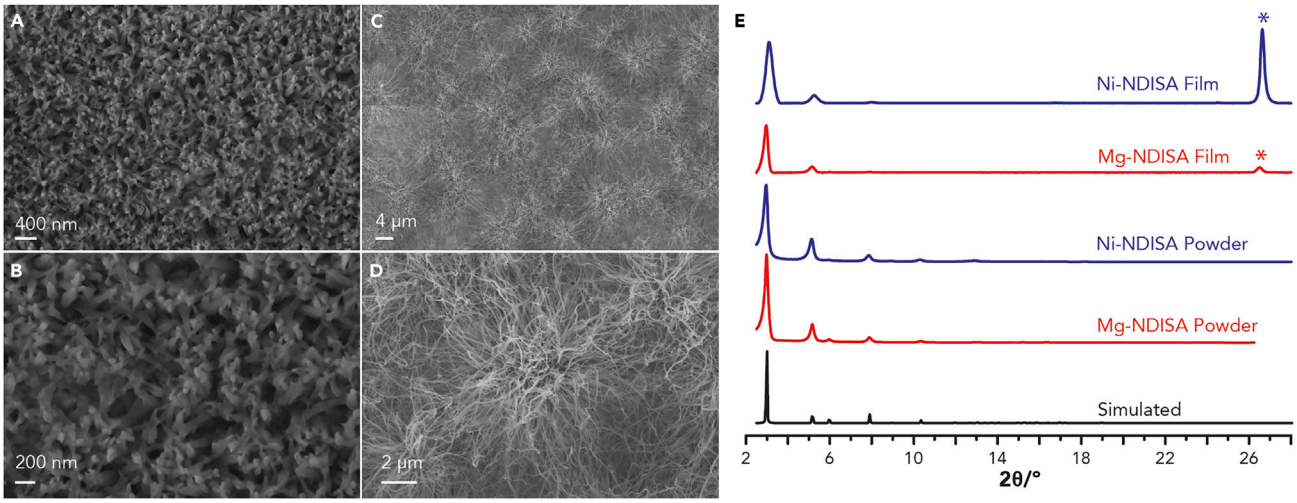

Figure 2. SEM Micrographs and PXRD Patterns of M-NDISA

(A–D) Scanning electron micrographs of (A and B) **Ni-NDISA** (at 400 and 200 nm magnifications, respectively) and (C and D) **Mg-NDISA** (at 4 and 2 μm magnifications, respectively) thin films. (E) Simulated and experimental PXRD patterns of **Mg-NDISA** and **Ni-NDISA** powders and thin films (peaks labeled with an asterisk correspond to FTO).

We sought to investigate the utility of **Mg-NDISA** and **Ni-NDISA** as electrochromic materials by measuring their absorption spectra during electrochemical cycling. Notably, because both materials can be deposited as thin films, both films are transparent when the NDI ligands are in their neutral state, and both turn dark upon reduction. However, because of their mesh- or fiber-like morphology, **Mg-NDISA** films exhibit significant scattering, which reduces their optical quality and therefore limits their practical applications (Figure S7). As such, spectroelectrochemical investigations were performed only on **Ni-NDISA** films, which exhibit no observable scattering. As shown in Figure S8, a UV-visible (UV-Vis) spectrum of the free ligand, H_4NDISA, in DMF closely matches that of **Ni-NDISA** films in their neutral state. Both are dominated by the strong $\pi \rightarrow \pi^*$ transitions of the NDI core, with λ_{max} at 362 and 383 nm. The **Ni-NDISA** film exhibited fast color changes at a constant potential of −2.0 V (versus Fc/Fc^+) (Figure 3). The absorption spectrum, collected at 1 s intervals, revealed the complete formation of $[NDI]^{\cdot-}$ species after 7 s, followed by the formation of doubly reduced $[NDI]^{2-}$ cores after an additional 23 s. The dark states of the reduced films are due to the intense absorptions across the visible spectrum centered at λ_{max} = 475, 700, and 772 nm for $[NDI]^{\cdot-}$ and 397, 423, and 560 nm for $[NDI]^{2-}$. We note that the width of the λ_{max} peak for NDI in its singly reduced state extends wider than it does in the doubly reduced state. Because the singly reduced state can be reached with an applied potential of only ~1 V in a two-electrode device, as expected from the CV in Figure S3, low power consumption can be expected for devices made from **Ni-NDISA**. Furthermore, because $[NDI]^{\cdot-}$ and $[NDI]^{2-}$ have almost complementary absorption profiles across the visible spectrum, **Ni-NDISA** films become nearly black at potentials where the ratio of $[NDI]^{\cdot-}$ to $[NDI]^{2-}$ is approximately 1:1 (see Figure 3 and Movies S1 and S2). Complete recovery of the transparent, neutral material upon application of an anodic potential confirms that the **Ni-NDISA** films exhibit fully reversible electrochromic behavior. Finally, the mesoporosity of **Ni-NDISA**, which is necessary for fast electrolyte transport within the material, was confirmed by measuring N_2 uptake isotherms on the activated bulk powder. As shown in Figure S9, **Ni-NDISA** displayed a type IV isotherm with high N_2 uptake at 77 K, consistent with the presence of mesoporous channels. Fitting

Table 1. Redox Potentials for Mg-NDISA, Ni-NDISA, and H_4NDISA

	$[NDI]/[NDI]^{\cdot-}$ $E_{1/2}$ (V)	$[NDI]^{\cdot-}/[NDI]^{2-}$ $E_{1/2}$ (V)
Mg-NDISA	−1.1	−1.7
Ni-NDISA	−1.2	−1.9
H_4NDISA	−1.0	−1.4

All potentials are reported versus Fc/Fc^+. See Figures S3 and S4 for CV curves.

the N_2 adsorption isotherm to the Brunauer-Emmett-Teller (BET) equation gave an apparent surface area of 1,722 ± 9 m^2/g, in line with previous MOF-74 analogs with similar pore sizes.[15]

DISCUSSION

Switching between the neutral and singly reduced state of **Ni-NDISA**, 7 s under our conditions, is faster than that of transition metal oxides (e.g., WO_3), which typically exhibit switching times of multiple seconds to minutes,[25–27] and is comparable with some of the reported polymeric electrochromic materials.[26,27] However, a reasonable comparison with other electrochromic materials can only be obtained in cases where the experimental setup and thin-film growth conditions are identical. We thus expect that it will be possible to improve the switching times for **Ni-NDISA** by optimizing the device construction, the electrolyte, and the quality of films. Although the intense absorption of the **Ni-NDISA** films caused deviations from a linear absorption response, thereby preventing the determination of a reliable coloration efficiency (CE), it is reasonable to assume that these films exhibit CE values similar to those reported for previous NDI-based electrochromic MOFs,[3] which exceeded 100 $cm^2\,C^{-1}$ in the blue region of the spectrum.

In conclusion, synthesis of a new salicylate-functionalized NDI ligand led to the isolation of two new mesoporous MOFs that have the MOF-74 topology and display ligand-based redox activity. We developed strategies for the deposition of thin films of Ni_2(NDISA) and Mg_2(NDISA), which exhibit morphologies that are highly dependent on their relative rates of nucleation and growth. **Ni-NDISA** films exhibit fast electrochromic switching from transparent to dark, a feature that is desirable for electrochromic materials and has potential applications in optoelectronic devices. Beyond electrochromism, our strategy for the formation of mesoporous MOFs bearing ligands with reversible multi-electron redox couples may find applications in energy-storage devices, especially when combined with redox-active metals.

EXPERIMENTAL PROCEDURES

CV

Measurements were carried out in a degassed DMF solution containing 0.1 M $[(nBu)_4N]PF_6$ using three-electrode electrochemical cells with the FTO substrate as the working electrode, platinum mesh as the counter electrode, and a platinum electrode (Pt disc) as the pseudo-reference electrode (calibrated against the Fc/Fc^+ couple). In order to ensure a stable potential from the pseudo-reference electrode, the films were cycled several times before the final CV was obtained and calibrated against the Fc/Fc^+ couple.

Spectroelectrochemistry

Measurements were conducted in a sealed transparent glass cell under a nitrogen flow in a degassed DMF solution containing 0.1 M $[(^nBu)_4N]PF_6$ using a three-electrode setup with the FTO substrate as the working electrode, platinum mesh as

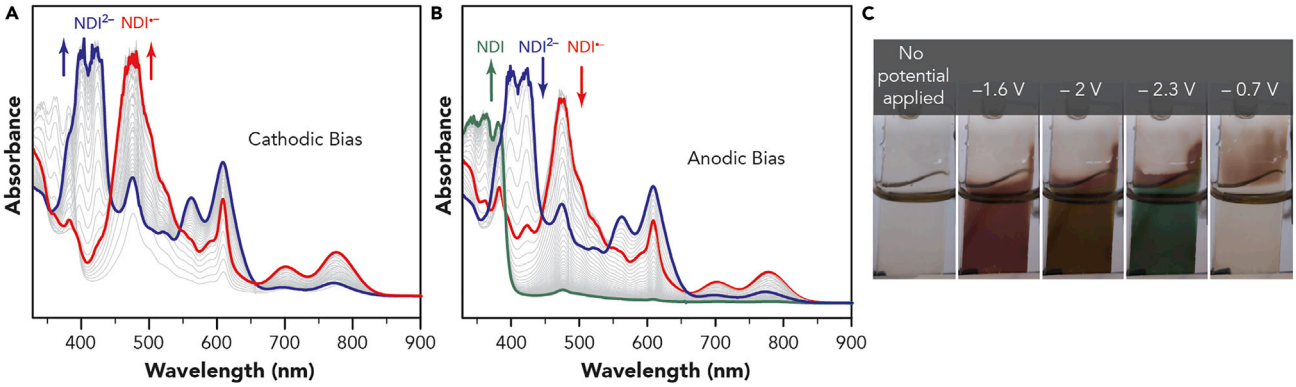

Figure 3. Spectroelectrochemical Analysis of Ni-NDISA

(A and B) Spectroelectrochemical data of **Ni-NDISA** collected by transmission UV-Vis spectroscopy show the reversible formation of $[NDI]^{\cdot-}$ and $[NDI]^{2-}$ when (A) −0.5 → −2 V reducing and (B) −2 → − 0.5 V oxidizing step potentials were applied (versus Fc/Fc^{+}).

(C) Images of reversible color switching of **Ni-NDISA** films at several reducing potentials (–1.6, –2, and −2.3 V versus Fc/Fc^{+}). Complete reversibility to the neutral transparent state was achieved by applying a reverse anodic bias (−0.7 V versus Fc/Fc^{+}). All measurements were performed in 0.1 M $[(^{n}Bu)_4N]PF_6$/DMF solution using a three-electrode setup, and the UV-Vis spectra were collected at 1 s intervals (see Experimental Procedures for details).

the counter electrode, and a platinum electrode (Pt disc) as the pseudo-reference electrode (calibrated against the Fc/Fc^{+} couple). The UV-Vis spectra of the **Ni-NDISA** films were obtained by applying a constant step potential from −0.5 to −2 V (versus Fc/Fc^{+}) and measuring the spectra at constant time intervals (1 s).

M-NDISA Structure Simulation

M-NDISA structures were simulated starting from the reported structure of IRMOF-74-IV.[15] NDISA was introduced in place of the original linker in the reported MOF, and the secondary building unit was modified to take into account the difference in connectives between NDISA and the original linker. No solvent molecules were included in the model. The unit cell parameters were then refined against the experimental pattern by Pawley refinement in Materials Studio (v.5.0.0.0, 2009; Accelrys Software). The simulated PXRD and structure are in the trigonal *R*3 space group; however, both *R*3 and $R\bar{3}$ space groups fit equally well. The pore diameter was then determined by measuring the van der Waals distance between two open-metal sites. Both **Mg-NDISA** and **Ni-NDISA** gave similar lattice parameters.

Gas-Sorption Measurements

Oven-dried sample tubes equipped with TranSeals (Micromeritics) were evacuated and tared. Samples were transferred to the sample tube, which was then capped by a TranSeal. The evacuated sample tubes were weighed again, and the sample mass was determined by subtracting the mass of the previously tared tubes. N_2 isotherms were measured with grade 5.0 N_2 gas using a liquid-nitrogen bath (77 K).

Synthesis of *N,N′*-Bis(3-carboxy-4-hydroxyphenyl)-1,4,5,8 Naphthalenetetradicarboximide

A dry 100 mL Schlenk flask was charged with 1,4,5,8-naphthalenetetracarboxylic dianhydride (1.0 g, 3.7 mmol), 5-amino-2-hydroxybenzoic acid (1.2 g, 7.8 mmol), and anhydrous DMF (35 mL) under a nitrogen atmosphere. The reaction mixture was heated at 130°C with rapid stirring for 1 day. The flask was cooled to room temperature, and the orange suspension was filtered off and washed with DMF, diethyl

ether, and methanol and then dried in vacuo to afford 1.5 g (70%) of orange powder. At this stage, the solid was isolated with one molecule of dimethyl amine ($HN(CH_3)_2$) per molecule of NDISA and was used in this form for further synthesis (the reported yield takes the presence of $HN(CH_3)_2$ into account). In order to obtain the pure form of the solid, an additional wash with ~30 mL of 2 M HCl for 1 day was necessary. ^{1}H NMR (400 MHz; dmso-d_6): δ 8.71 (4H, s), 8.35 (2H, s), 7.805 (2H, d, J = 2.8 Hz), 7.40 (2H, dd, J_1 = 8.6 Hz, J_2 = 2.4), 6.96 (2H, d, J = 8.4 Hz), 2.55 (6H, ($HN(CH_3)_2$), s). ^{13}C NMR (600 MHz; dmso-d_6): δ 171.16, 163.05, 161.68, 134.07, 130.49, 130.25, 126.96, 126.58, 125.11, 116.79, 116.49, 34.21 ($HN(CH_3)_2$). Elemental analysis calculated for $C_{30}H_{21}N_3O_4$: C, 61.71; H, 3.68; N, 7.30. Found: C, 61.39; H, 3.76; N, 7.15. This corresponds to a formula of $H_4NDISA \cdot HN(CH_3)_2$.

Synthesis of $[Mg_2(C_{28}H_{10}N_2O_{10})(H_2O)_2] \cdot 2.4(H_2O)$(Mg-NDISA) Powder

A 20 mL vial was charged with NDISA (55 mg, 0.094 mmol), $Mg(NO_3)_2 \cdot 6H_2O$ (80 mg, 0.31 mmol), and DMF/ethanol/water (7.5:0.5:0.5 mL). The reaction mixture was heated at 120°C for 1 day. After the reaction was allowed to cool to room temperature, the precipitated solids were separated by filtration and washed with DMF. The solids were then placed in 20 mL of methanol for 3 days; the solvent was decanted and refilled at least three times. The solids were then evacuated in a Tousimis Samdri PVT-3D critical-point dryer; the methanol-containing samples were completely exchanged with liquid CO_2. Then, the chamber containing the solids and liquid CO_2 was heated to 40°C to achieve supercritical conditions and held under those conditions for approximately 20 min. Finally, the chamber was slowly vented (20 min) to obtain crystalline solids. The samples were always kept solvated before the CO_2 drying step. Samples for combustion elemental analysis (C, H, and N) were heated to 40°C under a vacuum for 24 hr. Elemental analysis calculated for $Mg_2(C_{28}H_{18.8}N_2O_{14.4})$: C, 50.8; H, 2.86; N, 4.23. Found: C, 50.8; H, 2.79; N 4.13.

Synthesis of $[Ni_2(C_{28}H_{10}N_2O_{10})(H_2O)_2] \cdot 4(H_2O)$(Ni-NDISA) Powder

A 20 mL vial was charged with NDISA (55 mg, 0.094 mmol), $Ni(NO_3)_2 \cdot 6H_2O$ (104 mg, 0.36 mmol), and DMF/ethanol/water (7.5:0.5:0.5 mL). The reaction mixture was heated at 120°C for 1 day. After the reaction was allowed to cool to room temperature, the precipitated solids were separated by filtration and washed with DMF. The solids were then placed in 20 mL of methanol for 3 days; the solvent was decanted and refilled at least three times. The solids were then evacuated in a Tousimis Samdri PVT-3D critical-point dryer; the methanol-containing samples were completely exchanged with liquid CO_2. Then, the chamber containing the solids and liquid CO_2 was heated to 40°C to achieve supercritical conditions and held under those conditions for approximately 20 min. Finally, the chamber was slowly vented (20 min) to obtain crystalline solids. The samples were always kept solvated before the CO_2 drying step. Samples for combustion elemental analysis (C, H, and N) were placed under a high vacuum (10^{-6} torr) for 6 hr. Elemental analysis calculated for $Ni_2(C_{28}H_{22}N_2O_{16})$: C, 44.26; H, 2.92; N, 3.69. Found: C, 43.87; H, 2.27; N 3.46. Before the gas-adsorption measurement of **Ni-NDISA**, the sample was placed under a high vacuum (10^{-6} torr) at 100°C for 1 day.

Synthesis of M-NDISA Films on FTO, where M = Mg^{2+}, Ni^{2+}

H_4NDISA (55 mg, 0.094 mmol) and $Mg(NO_3)_2 \cdot 6H_2O$ (80 mg, 0.31 mmol) or $Ni(NO_3)_2 \cdot 6H_2O$ (90 mg, 0.31 mmol) were dissolved in anhydrous DMF (10 mL) and anhydrous methanol (1 mL) in a 20 mL vial. Precleaned FTO substrate (see general considerations in the Supplemental Information for details) was submerged in the solution with the conductive side facing downward. The solution was then heated to 120°C in a convection oven for 40 min in the case of **Mg-NDISA** and for 30 min

in the case of **Ni-NDISA**. All manipulations were done under ambient conditions. After the reaction was allowed to cool to room temperature, the substrates were removed, soaked, and washed with fresh DMF, and any solids attached to the non-conductive side were removed with a DMF-wet cotton swab. The substrates were then submerged in a vial containing methanol (20 mL) for at least 3 hr and up to 1 day before evacuation. The films were then evacuated in a Tousimis Samdri PVT-3D critical-point dryer (see the previous section for details on CO_2 drying). The samples were always kept solvated before the CO_2 drying step.

SUPPLEMENTAL INFORMATION

Supplemental Information includes general considerations, 11 figures, 1 table, 1 scheme, and 2 movies and can be found with this article online at http://dx.doi.org/10.1016/j.chempr.2016.06.013.

AUTHOR CONTRIBUTIONS

K.A. performed experiments. C.R.W. performed preliminary experiments with H_4NDISA. K.A. and M.D. devised experiments, interpreted data, and wrote the paper.

ACKNOWLEDGMENTS

Fundamental studies of opto-electronic properties of MOFs were supported by the Center for Excitonics, an Energy Frontier Research Center funded by the Basic Energy Sciences program of the US Department of Energy Office of Science (award no. DE-SC0001088 to the Massachusetts Institute of Technology [MIT]). Translational support for developing smart windows from electrochromic MOFs was provided by a cooperative agreement between the Masdar Institute of Science and Technology (Abu Dhabi) and MIT (reference 02/MI/MIT/CP/11/07633/GEN/G/00). K.A. acknowledges Saudi Aramco for financial support during graduate studies. We thank Dr. M.G. Campbell and Dr. D. Sheberla for insightful discussions. We thank Dr. D. Sheberla for assistance with image processing and Dr. Y. Tulchinsky for assistance with ^{13}C NMR.

Received: March 26, 2016
Revised: April 28, 2016
Accepted: May 19, 2016
Published: August 11, 2016

REFERENCES AND NOTES

1. Kornienko, N., Zhao, Y., Kley, C.S., Zhu, C., Kim, D., Lin, S., Chang, C.J., Yaghi, O.M., and Yang, P. (2015). Metal–organic frameworks for electrocatalytic reduction of carbon dioxide. J. Am. Chem. Soc. *137*, 14129–14135.

2. Ahrenholtz, S.R., Epley, C.C., and Morris, A.J. (2014). Solvothermal preparation of an electrocatalytic metalloporphyrin MOF thin film and its redox hopping charge-transfer mechanism. J. Am. Chem. Soc. *136*, 2464–2472.

3. Wade, C.R., Li, M., and Dincă, M. (2013). Facile deposition of multicolored electrochromic metal–organic framework thin films. Angew. Chem. Int. Ed. Engl. *52*, 13377–13381.

4. Garai, B., Mallick, A., and Banerjee, R. (2016). Photochromic metal–organic frameworks for inkless and erasable printing. Chem. Sci. *7*, 2195–2200.

5. Usov, P.M., Fabian, C., and D'Alessandro, D.M. (2012). Rapid determination of the optical and redox properties of a metal–organic framework *via in situ* solid state spectroelectrochemistry. Chem. Commun. (Camb.) *48*, 3945–3947.

6. Kung, C.W., Wang, T.C., Mondloch, J.E., Fairen-Jimenez, D., Gardner, D.M., Bury, W., Klingsporn, J.M., Barnes, J.C., Van Duyne, R., Stoddart, J.F., et al. (2013). Metal−organic framework thin films composed of free-standing acicular nanorods exhibiting reversible electrochromism. Chem. Mater. *25*, 5012–5017.

7. D'Alessandro, D. (2016). Exploiting redox activity in metal–organic frameworks: concepts, trends and perspectives. Chem. Commun. (Camb.) *52*, 8957–8971.

8. Stavila, V., Talin, A.A., and Allendorf, M.D. (2014). MOF-based electronic and opto-electronic devices. Chem. Soc. Rev. *43*, 5994.

9. Kobayashi, Y., Jacobs, B., Allendorf, M.D., and Long, J.R. (2010). Conductivity, doping, and redox chemistry of a microporous dithiolene-based metal−organic framework. Chem. Mater. *22*, 4120–4122.

10. Sun, L., Campbell, M.G., and Dincă, M. (2016). Electrically conductive porous metal–organic frameworks. Angew. Chem. Int. Ed. Engl. *55*, 2–16.

11. Jeon, I.-R., Sun, L., Negru, B., Van Duyne, R.P., Dincă, M., and Harris, T.D. (2016). Solid-state redox switching of magnetic exchange and electronic conductivity in a

benzoquinoid-bridged Mn^{II} chain compound. J. Am. Chem. Soc. *138*, 6583–6590.

12. Shekhah, O., Liu, J., Fischer, R.A., and Wöll, C. (2011). MOF thin films: existing and future applications. Chem. Soc. Rev. *40*, 1081–1106.

13. Bradshaw, D., Garai, A., and Huo, J. (2012). Metal–organic framework growth at functional interfaces: thin films and composites for diverse applications. Chem. Soc. Rev. *41*, 2344–2381.

14. Allendorf, M.D., Schwartzberg, A., Stavila, V., and Talin, A.A. (2011). A roadmap to implementing metal-organic frameworks in electronic devices: challenges and critical directions. Chem. Eur. J. *17*, 11372–11388.

15. Deng, H., Grunder, S., Cordova, K.E., Valente, C., Furukawa, H., Hmadeh, M., Gandara, F., Whalley, A.C., Liu, Z., Asahina, S., et al. (2012). Large-pore apertures in a series of metal-organic frameworks. Science *336*, 1018.

16. Kapelewski, M.T., Geier, S.J., Hudson, M.R., Stück, D., Mason, J.A., Nelson, J.N., Xiao, D.J., Hulvey, Z., Gilmour, E., FitzGerald, S.A., et al. (2014). M_2(m-dobdc) (M = Mg, Mn, Fe, Co, Ni) Metal–organic frameworks exhibiting increased charge density and enhanced H_2 binding at the open metal sites. J. Am. Chem. Soc. *136*, 12119–12129.

17. Cozzolino, A.F., Brozek, C.K., Palmer, R.D., Yano, J., Li, M., and Dincă, M. (2014). Ligand redox non-innocence in the stoichiometric oxidation of Mn 2(2,5-dioxidoterephthalate) (Mn-MOF-74). J. Am. Chem. Soc. *136*, 3334–3337.

18. Aubrey, M.L., and Long, J.R. (2015). A dual–ion battery cathode via oxidative insertion of anions in a metal–organic framework. J. Am. Chem. Soc. *137*, 13594–13602.

19. Suraru, S.-L., and Würthner, F. (2014). Strategies for the synthesis of functional naphthalene diimides. Angew. Chem. Int. Ed. Engl. *53*, 7428–7448.

20. Bhosale, S.V., Jani, C.H., and Langford, S. (2008). Chemistry of naphthalene diimides. J. Chem. Soc. Rev. *37*, 331–342.

21. Guha, S., Goodson, F.S., Corson, L.J., and Saha, S. (2012). Boundaries of anion/naphthalenediimide interactions: from anion–π interactions to anion-induced charge-transfer and electron-transfer phenomena. J. Am. Chem. Soc. *134*, 13679–13691.

22. Takashima, Y., Martinez, V.M., Furukawa, S., Kondo, M., Shimomura, S., Uehara, H., Nakahama, M., Sugimoto, K., and Kitagawa, S. (2011). Molecular decoding using luminescence from an entangled porous framework. Nat. Commun. *2*, 168.

23. Mallick, A., Garai, B., Addicoat, M.A., Petkov, P.S., Heine, T., and Banerjee, R. (2015). Solid state organic amine detection in a photochromic porous metal organic framework. Chem. Sci. *6*, 1420–1425.

24. The structure can be simulated equally well in space groups *R*3 and $R\bar{3}$.

25. Monk, P.M.S., Mortimer, R.J., and Rosseinsky, D.R. (2007). Electrochromism and Electrochromic Devices (New York: Cambridge University Press).

26. Beaujuge, P.M., Ellinger, S., and Reynolds, J.R. (2008). The donor-acceptor approach allows a black-to-transmissive switching polymeric electrochrome. Nat. Mater. *7*, 795.

27. Hsu, P.-C., Wang, S., Narasimhan, V.K., Kong, D., Lee, H.R., and Cui, Y. (2013). Performance enhancement of metal nanowire transparent conducting electrodes by mesoscale metal wires. Nat. Commun. *4*, 2522.